JOURNAL OF GEOPHYSICAL RESEARCH, VOL. 102, NO. D22, PAGES 25,751–25,762, NOVEMBER 27, 1997

Impact of the Doppler spread parameterization on the simulation of the middle atmosphere circulation using the MA/ECHAM4 general circulation model

E. Manzini

Max Planck Institut für Meteorologie, Hamburg, Germany

N. A. McFarlane

Canadian Centre for Climate Modelling and Analysis, Victoria, British Columbia, Canada

C. McLandress[1]

Institute for Space and Terrestrial Science, North York, Ontario, Canada

Abstract. The zonal mean circulation of the middle atmosphere simulated by a general circulation model that includes the Doppler spread parameterization of gravity-wave momentum deposition is presented. To illustrate the impact of the parameterization, this simulation is compared to another obtained by using Rayleigh friction instead. It is found that the Doppler spread parameterization improves the extratropical zonal mean circulation in the mesosphere by reducing the strength of the zonal winds above the jet maximum. The parameterization also improves the simulation of the equatorial semiannual oscillation in the zonal mean zonal wind at the stratopause by enhancing the eastward phase and its downward propagation.

1. Introduction

The current interest in understanding the effects of changes in the chemical composition of the atmosphere motivates the development of general circulation models (GCMs) which are capable of simulating the global transport and evolution of the atmospheric constituents in the troposphere and stratosphere. Existing models of this type have generally evolved from global circulation models of the troposphere. Consequently, they have realistic representations of the large-scale processes that govern the troposphere, including the forcing of the vertically propagating planetary waves that account for a significant amount of the extratropical variability in the middle atmosphere. Such models, however, are known to exhibit significant biases in the zonally averaged circulation of the middle atmosphere, especially in the southern hemisphere winter and spring, when the simulated zonal mean winds are extremely strong [*Hamilton et al.*, 1995; *Boville*, 1995; *Manzini and Bengtsson*, 1996]. It is now generally recognized that simulations of the middle atmosphere can be greatly improved by taking into account the momentum deposition associated with upward propagating gravity waves (see *Andrews et al.*, [1987] for a review). Given that current state-of-the-art middle atmosphere GCMs do not explicitly resolve these small-scale waves, it is therefore of primary importance to develop and test parameterizations of their effects on the large-scale circulation.

Until recently, most GCMs have included only parameterizations of the momentum deposition from orographic gravity waves [e.g., *McFarlane*, 1987; *Miller et al.*, 1989]. Orographically excited gravity waves (which are stationary) have been shown to play an important role in the extratropical regions of the northern hemisphere middle atmosphere during winter [*Boville*, 1991, 1995]. Gravity waves with nonzero phase speeds relative to the surface make a significant and possibly predominant contribution to the momentum budget of the northern hemisphere extratropics during summer and in the tropics and southern hemisphere at all times of year.

The parameterizations of gravity-wave momentum deposition used so far have been based exclusively on upward propagating linear, monochromatic waves and their dissipation due to onset of static instabilities associated with wave amplitude growth with height. The linear wave saturation mechanism of momentum deposition [*Lindzen*, 1981] treats each wave of a chosen discrete spectrum in isolation. There is now consider-

[1]Now at University of Washington. Seattle, Washington

Paper number 97JD01096.
0148-0227/97/97JD-01096$09.00

able evidence to support the existence of a continuous and nearly universal spectrum of vertically propagating gravity waves in the middle atmosphere. The nearly universal nature of the spectrum has been ascribed to a variety of saturation processes (*Fritts* [1984, 1989] for reviews). These include the linear instability of a continuous spectrum [*Dewan and Good*, 1986; *Smith et al.*, 1987] and the combined effects of nonlinear interactions among the waves and dissipation associated with the onset of instability [*Hines*, 1991a, b, c, 1993; *Medvedev and Klassen*, 1995].

Recently, *Hines* [1997a, b] has proposed a parameterization of gravity-wave momentum deposition based on the Doppler spread theory which is suitable for use in general circulation models. The theory assumes the existence of a continuous spectrum of gravity waves which propagate upward from the troposphere, where they are generated by a variety of processes, including convective activity, frontal systems, and unsteady flow over orography. In addition to being Doppler shifted by the large-scale background wind, each wave component of the spectrum is also affected by the wind field induced by the other waves. In the Doppler spread theory this nonlinear interaction gives rise, in a statistical sense, to a spreading of the vertical wavenumber spectrum toward high wavenumbers, where dissipation and momentum deposition occur.

The purpose of this paper is to test the Doppler spread parameterization in a middle atmosphere general circulation model. Given the exploratory character of this work, a relatively low horizontal resolution version of the GCM has been used. This resolution is adequate, however, to reveal the benefits of using this parameterization, as supported by more recent results at higher horizontal resolution [*Manzini et al.*, 1997; *McFarlane and Manzini*, 1997].

Another simulation performed with the same GCM, but with Rayleigh friction in the mesosphere instead of the Doppler spread parameterization, is used as the control integration for comparison. In the present paper, attention is restricted to the effects of nonorographic gravity waves. Therefore an explicit parameterization of the orographic gravity wave drag is not included.

The paper is arranged in the following manner: The general circulation model and the Doppler spread parameterization are described in section 2. General results for the zonal mean circulation in January and July are presented in section 3, while section 4 deals with the behavior in the tropical middle atmosphere. Conclusions are discussed in section 5.

2. Model and Experiments

The model used is the middle atmosphere (MA) version of the ECHAM4 general circulation spectral transform model with state-of-the-art physical parameterizations, developed at the Max Planck Institute. The MA/ECHAM4 model is the upward extension of the original ECHAM4 GCM with top at 10 hPa (about 30 km). The salient features of the ECHAM4 model [*Roeckner et al.*, 1996a, b and reference therein] are here briefly summarized: radiation scheme based on the ECMWF scheme [*Morcrette*, 1991] and modified by *Giorgetta and Wild* [1995]; prognostic scheme for stratiform clouds [*Roeckner et al.*, 1991]; mass flux scheme for cumulus and stratocumulus convection, including deep, midlevel and shallow convection based on *Tiedtke* [1989]; nonlocal vertical diffusion scheme [*Brinkop and Roeckner*, 1995]; three layer model of heat conduction and soil model [*Blondin*, 1989; *Dümenil and Todini*, 1992]; and semiLagrangian transport for water vapor, liquid water, and tracers [*Williamson and Rasch*, 1994].

The MA/ECHAM4 general circulation model has 39 vertical levels and extends from the surface to 0.01 hPa (about 80 km). In the lower stratosphere the vertical resolution is about 1.5 km and slowly decreases with height to about 6-7 km at the model top. Other modifications to the troposphere version of the model follow *Manzini and Bengtsson* [1996]. They include a simple implementation of the Voigt effect at low pressure in the radiation scheme, an ozone distribution from the monthly zonal mean distribution of a chemical model, and a ∇^4 linear operator for the horizontal diffusion.

In the standard version of the MA/ECHAM4 model, Rayleigh friction is used to dissipate resolved upward propagating waves and also to act as a crude parameterization of the effects of gravity wave drag on the zonal mean flow in the mesosphere, a procedure that is commonly used in middle-atmosphere models. The Rayleigh friction coefficient increases upward from $(32\ \text{days})^{-1}$ at 0.4 hPa (six levels from the top) to $(1\ \text{day})^{-1}$ at 0.01 hPa (the model top). The simulation performed with this configuration is referred to as the RFD experiment.

In the simulation using the Doppler spread parameterization the Rayleigh friction is removed. This latter simulation is referred to as the DSP experiment.

Both the RFD and DSP versions employed monthly mean climatological sea surface temperature [*Gates*, 1992] and the seasonal and diurnal cycle in the radiative transfer scheme. Both have been integrated for a total of 4 years at T21 horizontal truncation. Note that both simulations were performed without any orographic gravity wave drag parameterization.

2.1. Doppler Spread Parameterization

The formulation of the Doppler spread parameterization follows *Hines* [1997a, b]. The gravity waves are assumed to propagate upward from the troposphere, where they are generated, and to interact nonlinearly with each other. The nonlinearity considered here is associated with horizontal advection, which statistically spreads the vertical wavenumber spectrum preferentially toward high wavenumbers. As the waves propagate upward, wave action density is conserved until the gravity wave spectrum as a whole becomes unsta-

ble and the waves at high vertical wavenumbers break down into turbulence. It is assumed that these waves are removed from the spectrum and that the momentum carried by them is deposited into the background flow. At any given height, the vertical wavenumber at which the wave breakdown begins can be expressed in terms of a corresponding wavenumber (referred to as the cutoff wavenumber) of the gravity wave spectrum at the surface (initial height). In the notation of *Hines* [1997b], for a given azimuth (j) and height, the cutoff wavenumber is given by

$$m_j = N_i[\Phi_1\sigma_j + \Phi_2\sigma_h + V_j - V_{ji}]^{-1} \quad (1)$$

where N_i is the buoyancy frequency at the initial height, σ_h is the total rms horizontal wind speed induced by the gravity waves, σ_j is the rms horizontal wind speed in the j azimuth, Φ_1 and Φ_2 are constants ("fudge" factors constrained by the theory), V_j is the background wind in the j azimuth, and V_{ji} is the background wind in the j azimuth at the initial height. The first term on the right-hand side of (1) represents the effect of Doppler shifting by the gravity-wave-induced wind; the second term is derived from the condition for the onset of instability of the total wave system; and the third term represents the effect of Doppler shifting by the background flow. The momentum deposition is deduced from the vertical variation of the cutoff wavenumber m_j, under the constraint that m_j be positive and nonincreasing with height. This constraint can be achieved, because there always exists a positive m_j at the initial height (where $V_j - V_{ji}$ is zero).

The parameters used in the current version of the Doppler spread parameterization are summarized in Table 1. These include the specification at the initial height of the slope of the vertical wavenumber spectrum at low wavenumbers, which is assumed to follow a power law, and the gravity-wave-induced rms wind speed, chosen to give values at the tropopause in reasonable accord with available estimates of gravity wave variances [e.g., *Fritts and Nastrom*, 1992; *Allen and Vincent*, 1995]. In the parameterization version used here, a geographically uniform isotropic gravity wave spectrum is assumed to be launched at the surface (initial height).

In the current application the contribution to the vertical diffusion that arises from the gravity-wave momentum deposition has not been included and the gravity-wave momentum flux at the upper boundary of the model (formally pressure equal to zero) is set to zero. In another recent application of the Doppler spread parameterization in a general circulation model that extends above 80 km [*McFarlane et al.*, 1997], a low wavenumber bound to the initial vertical wavenumber spectrum has been introduced to limit the amount of drag in the lower thermosphere (where the spectrum may, in fact, no longer be broad) and to avoid numerical difficulties arising from a positive feedback between the Doppler spread parameterization and the diurnal tide [*McLandress*, 1997]. In the MA/ECHAM4 model these numerical difficulties do not appear, presumably because the top is below the height where the diurnal tide maximizes (near 90 km). Consequently, the low-wavenumber bound has not been introduced.

3. Zonal Mean Circulation

The 4 year average zonal mean zonal wind and temperature fields for January and July from the DSP simulation and the CIRA86 reference atmosphere [*Fleming et al.*, 1990] are shown in Figures 1 and 2, respectively. Although the CIRA86 data set is based on only a few years of middle-atmosphere data, and so may not be truly indicative of the long-term mean state, it nevertheless provides a useful reference. The simulated easterlies in the summer middle atmosphere of both hemispheres exhibit a realistic structure, with the strongest winds occurring in the subtropical upper mesosphere. In qualitative agreement with the CIRA86 reference atmosphere the summer easterlies in the DSP simulation are seen to extend into the winter hemisphere at the stratopause, while westerlies prevail in the equatorial mesosphere. The DSP summer easterlies though are somewhat weaker in the upper mesosphere, especially in July. For both winter hemispheres the simulated mean zonal wind differs significantly from that of CIRA86, notably with respect to the excessive strength of the westerlies in the stratosphere and the confinement of the mesospheric eastward jet to high latitudes. Given that the DSP simulation did not include orographic gravity

Table 1. Parameter Setting for the DSP simulation

Parameter	Description
$s = 1$	slope of the vertical wavenumber spectrum at the initial height (surface)
$\sigma_{hi} = 1.5$ ms^{-1}	rms horizontal wind speed at the initial height
$K^* = 7 \times 10^{-6}$ m^{-1}	effective horizontal wavenumber
$J = 8$	number of equally spaced azimuths
$\Phi_1 = 1.5$	directional rms coefficient
$\Phi_2 = 0.3$	total rms coefficient

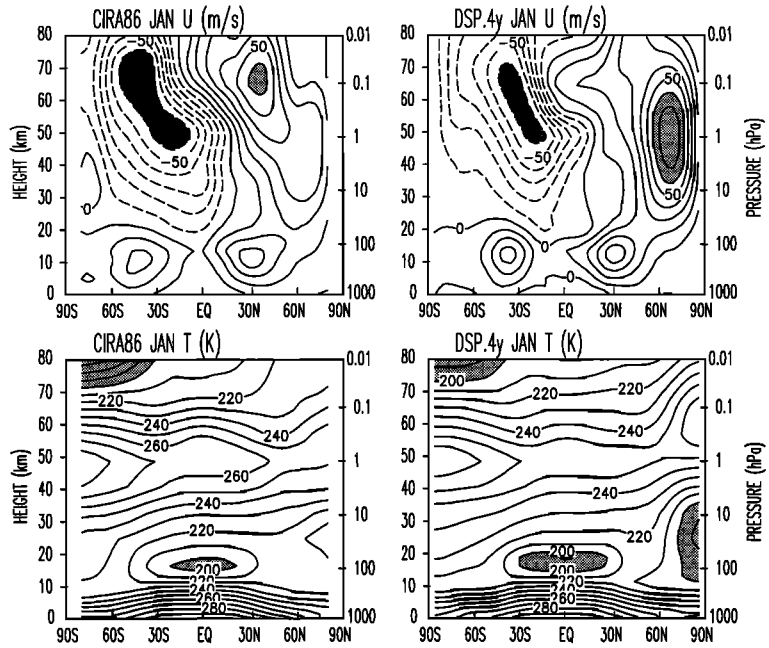

Figure 1. January zonal mean zonal wind (ms^{-1}, top) and temperature (K, bottom) from CIRA86 (left) and from the 4 year DSP simulation (right). The contour interval is 10 ms^{-1} for the zonal winds (< -60, dark shading; > 60, light shading) and 10 K for the temperatures (< 200, light shading). In this and the following figures, the height on the left of each plot is the log-pressure vertical coordinate obtained by using a scale height $H = 7$ km.

wave drag, the strong winds in the northern hemisphere winter are not unexpected [*Boville*, 1991, 1995]. The July zonal wind bias in the southern hemisphere lower stratosphere is in part due to a deficient representation of the troposphere in a T21 simulation [*Manzini and Bengtsson*, 1996], typically producing a meridionally narrower subtropical tropospheric jet.

While the general structure of the zonal mean temperature (Figures 1 and 2, bottom panels) is captured by the DSP simulation, a cold bias in the winter strato-

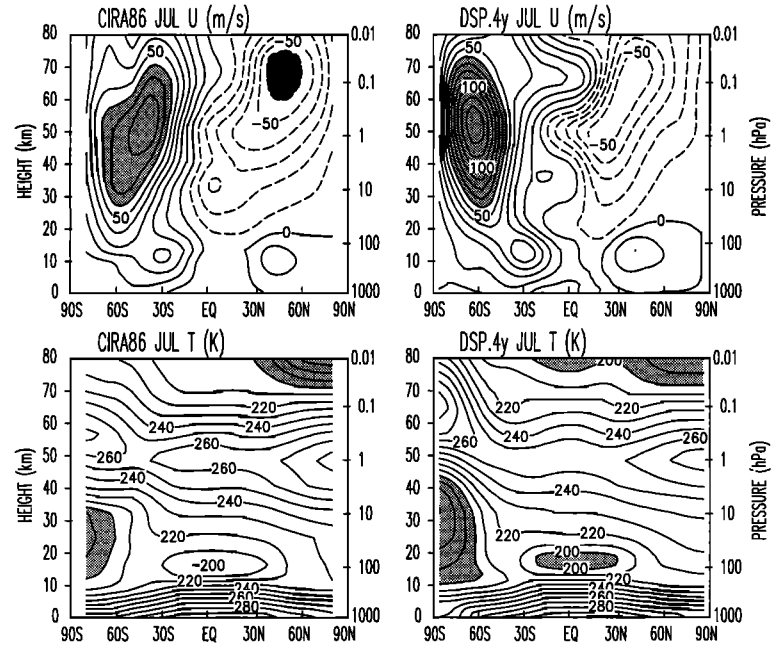

Figure 2. July zonal mean zonal wind (ms^{-1}, top) and temperature (K, bottom) from CIRA86 (left) and from the 4 year DSP simulation (right). The contour interval is 10 ms^{-1} for the zonal winds (< -60, dark shading; > 60, light shading) and 10 K for the temperatures (< 200, light shading).

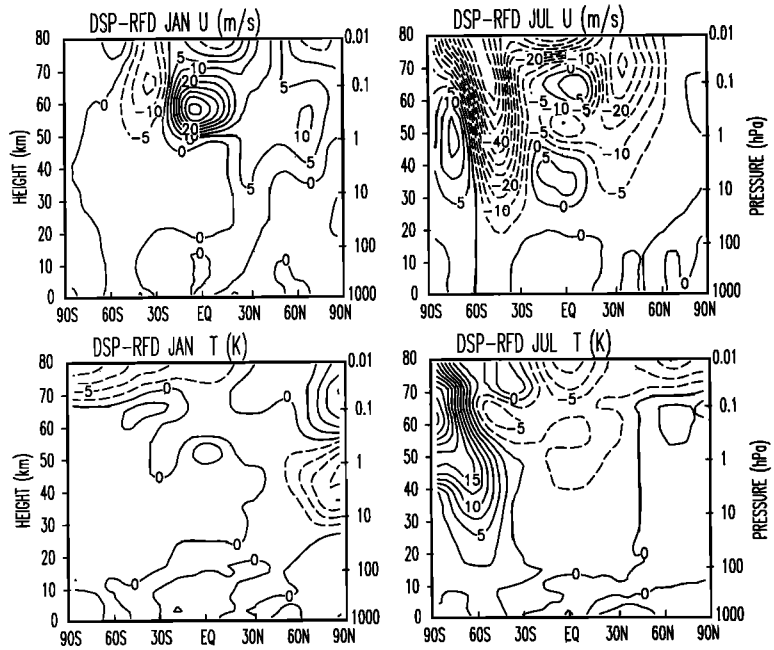

Figure 3. Difference between the DSP and the RFD simulations, DSP-RFD, for the 4 year average of the zonal mean zonal wind (ms^{-1}, top) and the temperature (K, bottom), January at left and July at right. The contour interval is 5 ms^{-1} for the zonal winds and 2.5 K for the temperatures.

sphere and an associated upward shift of the stratopause is apparent in both hemispheres. This cold bias is particularly severe in the southern hemisphere winter. In summer the simulated stratopause is located at 1 hPa, in agreement with CIRA86, although about 10 K colder. In the mesosphere, the summer zonal mean temperature decreases with height, in accord with observations albeit at a slower rate. Consequently, the simulated zonal mean temperature is too warm by about 20 K at the summer pole near the model top.

It is noteworthy that the CIRA86 data may also have a warm bias in the summer mesopause region. This is suggested by the observations of *Lübken and van Zahn* [1991] which indicate that in summer the temperature at 88 km in the polar region is about 15 K colder than the CIRA86 analysis. This level is, however, above the uppermost level of the MA/ECHAM4 model.

To improve the simulation of the upper mesosphere, it is most likely necessary to raise the upper boundary of the model. The results of *McFarlane et al.*, [1997], in which the DSP has been implemented in a GCM with a top at approximately 97 km, indicate that the summer polar submesopause temperatures are, in fact, in better agreement with both CIRA86 and *Lübken and van Zahn* [1991].

To highlight the impact of the DSP on the simulation of the middle atmosphere circulation in January and July, the differences between the DSP and the RFD simulations (DSP-RFD) for the mean zonal wind and temperature are shown in Figure 3. In the troposphere the winds and temperature fields do not appear to differ significantly, suggesting that the zonal mean tropospheric circulation is not substantially affected by the specification of the mechanism of momentum dissipation in the mesosphere.

In January (Figure 3, top left) the most notable feature is a large positive difference in the zonal mean wind found in the equatorial mesosphere. This difference ($\sim$40 ms^{-1}) is caused by the appearance of westerlies in the DSP simulation, while easterlies or weak westerlies dominate the flow in the RFD simulation in the equatorial mesosphere. Differences of about 10-15 ms^{-1} are also found in July (Figure 3, top right) in the equatorial middle atmosphere. As will be shown in section 4, the behavior of the DSP experiment at the equator is associated with an enhancement of the simulated semiannual oscillation in the zonal mean zonal wind at the stratopause.

The mean zonal wind and temperature differences found in January in the northern hemisphere indicate that in the lower mesosphere and upper stratosphere the DSP extratropical westerlies are about 5-10 ms^{-1} stronger at high latitudes, consistent with the colder polar stratosphere and an upward shift of the stratopause (Figure 3, bottom left). A longer integration, however, would be necessary to highlight any possible statistically significant difference during the northern hemisphere winter, because of the large interannual variability there [*Boville*, 1995; *Hamilton*, 1995; *Manzini and Bengtsson*, 1996]. Moreover, other processes, such as orographic gravity wave drag and the model's horizontal resolution may impact more significantly on the northern hemisphere winter circulation.

It is interesting to note that although the DSP west-

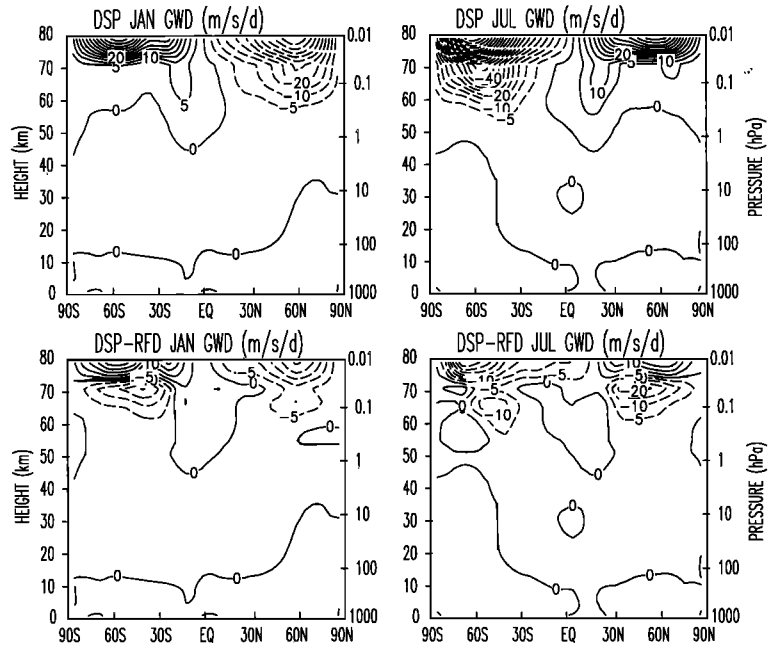

Figure 4. Zonal mean zonal drag from the 4 year DSP simulation ($ms^{-1}d^{-1}$, top). Difference between the DSP and RFD simulations, DSP-RFD, for the 4 year average of the zonal mean zonal drag ($ms^{-1}d^{-1}$, bottom). January at left and July at right. The contour interval is 5 $ms^{-1}d^{-1}$.

erlies are stronger than the RFD winds, they actually decrease slightly more rapidly with height in the upper mesosphere in the northern hemisphere winter, as indicated by the negative difference at the model top there. This is also clearly apparent in the southern hemisphere winter. Figure 3 (top right) shows that in the stratosphere at 60°S the difference in zonal wind is small (zero contour), indicating that the magnitude of the eastward jet is similar in the two experiments. At 1 hPa the DSP winter jet is confined more poleward (positive difference south of 60°S), while above 0.1 hPa, the difference in zonal wind is negative also at high latitudes and attains a value of 55 ms^{-1} near 55°S at the model top, indicating that much weaker winds (by a factor of 2) characterize the DSP upper mesosphere. These results therefore indicate that the Doppler spread parameterization is more effective than Rayleigh friction (as used here) in reducing the magnitude of the zonal mean winds. In the southern hemisphere winter, the change in zonal wind is associated with a positive temperature difference throughout most of the high-latitude middle atmosphere (Figure 3, bottom right).

In July the northern hemisphere easterlies are stronger in the subtropical middle mesosphere in the DSP simulation. A similar result is found in the southern hemisphere in January. The zonal mean temperature difference field is consistent with these changes, being negative at the summer pole in the upper mesosphere. Note that both experiments exhibit mean mesospheric temperatures that are in qualitative agreement with observations and that depart from the radiatively determined temperature [*Fels*, 1985] in the sense expected; namely, they are warmer in winter and colder in summer. Therefore the temperature change shown in Figure 3 implies that in the upper mesosphere the DSP temperature field departs more from the radiatively determined temperature and that the DSP residual mean meridional circulation is stronger (not shown). The opposite occurs in the stratosphere and lower mesosphere, with the exception of the southern hemisphere winter, where the temperature difference is positive also in the stratosphere.

Figure 4 shows the 4 year average of the zonal mean zonal gravity wave drag from the DSP experiment (top panels) and the difference between the DSP and RFD experiments (bottom panels). In summer at extratropical latitudes the DSP gravity wave drag is smaller than the Rayleigh friction drag in the lower and middle mesosphere but larger than the RFD drag in the upper mesosphere. In the summer hemisphere the mean temperature field response shown in Figure 3 (bottom panels) is consistent with the expectation from the "downward control" mechanism [*Haynes et al.*, 1991], in that a stronger (weaker) drag should be associated with a stronger (weaker) residual mean meridional circulation and result in temperatures being farther away from (closer to) radiative equilibrium. In the southern hemisphere winter, the DSP drag is larger than the RFD drag throughout most of the mesosphere, which is presumably the cause of the warmer temperature and much weaker zonal wind in the DSP experiment. The DSP drag is also larger in the northern hemisphere winter.

However, the contribution of the resolved waves to the eddy forcing of the zonal mean zonal wind (not shown) is not negligible there, so that the total drag is actually reduced at high latitudes in the northern hemisphere lower mesosphere in January in the DSP case. The colder temperatures in the DSP upper polar stratosphere (Figure 3 bottom left) are consistent with such a total zonal drag difference field. The contribution from the resolved waves is generally much smaller than that from the parameterized drag in the other seasons.

4. Semiannual Oscillation at the Stratopause

Evidence of a semiannual oscillation (SAO) in the zonal wind and temperature fields at the equatorial stratopause was established several decades ago by radiosonde and rocket measurements [*Reed*, 1962, 1965, 1966; *Belmont et al.*, 1974, 1975] and reviewed by *Hirota* [1980]. The predominant features of the zonal wind oscillation are the occurrence of easterlies (westerlies) one month after the solstice (equinox), downward propagation of the wind regimes (less pronounced for the easterlies), and a 20-30 ms^{-1} amplitude maximum at 45-50 km located just south of the equator. The temperature oscillation also exhibits a downward propagation, with the largest amplitude (several degrees) occurring at 35-40 km, slightly below the amplitude maximum

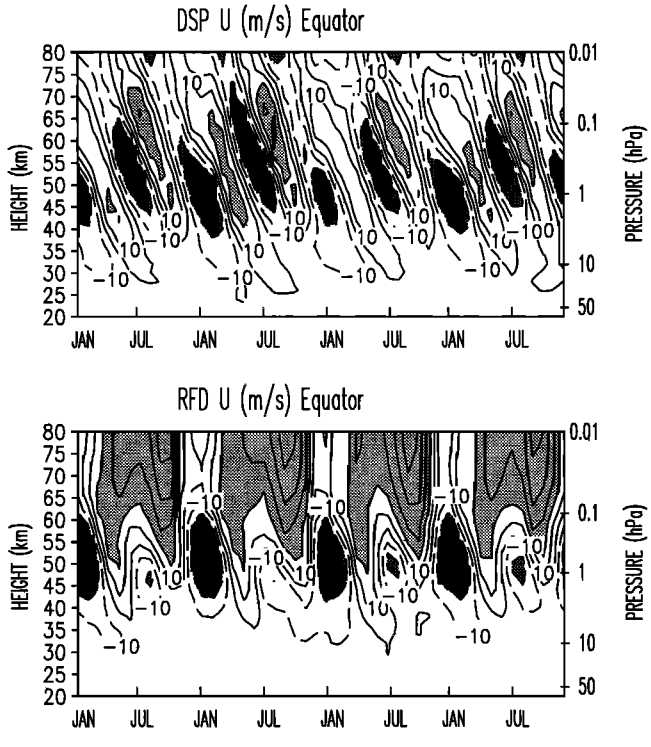

Figure 5. Time-height section of the zonal mean zonal wind (ms^{-1}) at the equator from the DSP simulation (top) and the RFD simulation (bottom). The contour interval is 10 ms^{-1} (< -20, dark shading; > 20, light shading).

in the zonal wind and in accordance with thermal wind balance. The SAO is also know to exhibit a pronounced seasonal variation. The cycle from January to April, the so-called first cycle, is characterized by stronger easterlies and westerlies than in the second cycle, from July to October [*Belmont et al.*, 1975]. Seasonal variations in the temperature oscillation have also been reported from satellite measurements by *Delisi and Dunkerton* [1988].

The time evolution of the monthly averaged zonal mean zonal wind at the equator during the 4 years of model simulation for the two experiments is presented in Figure 5. Throughout the entire middle atmosphere, alternating regimes of easterlies and westerlies propagate downward in the DSP experiment (Figure 5, top panel). At 1 hPa the winds are westward in January and July and eastward after the equinox (April and October). Considerable interannual variability is also apparent in the DSP zonal winds at the equator. For instance, a rather strong double cycle is seen during the second year, followed by a particularly weak January to April cycle. In the stratosphere, below 1 hPa, the first cycle (January to April) is occasionally slightly stronger, while in the mesosphere, the westerlies of the second cycle tend to be larger. In the middle mesosphere the long-term average zonal winds at the equator (not shown) are eastward between 55 and 75 km and westward above, in qualitative agreement with observations [*Dunkerton*, 1982; *Hamilton*, 1982].

We turn now to the RFD experiment. In the vicinity of the 1 hPa level there is a semiannual oscillation (Figure 5, bottom panel), although there is very little evidence of downward propagation. The first cycle of the oscillation is clearly stronger, with the January easterlies being about twice that of July. In addition the July easterlies are confined to the region below 55 km. The westerlies are mainly confined to the mesosphere and in April and October do not descend below 45 km. Westerlies are, in fact, dominant throughout all the mesosphere and at the model top in the long-term mean. The RFD semiannual oscillation appears to be similar in character to that obtained with other general circulation models that do not employ parameterizations of the effects of a spectrum of gravity waves [*Sassi et al.*, 1993; *Hamilton et al.*, 1995]. The occurrence of stronger easterlies in January in the MA/ECHAM4 model is also found in those other model results and is associated with the meridional advection of momentum by the residual mean meridional circulation, expected to be stronger during the northern hemisphere winter. See, for instance, *Delisi and Dunkerton* [1988], for a discussion of the seasonal variations of the semiannual oscillation at the stratopause.

The simulated oscillations are further compared in Figure 6, which shows the zonal wind semiannual amplitude and phase distributions. In both experiments, near the 1 hPa level the semiannual amplitude is largest at the equator, with an amplitude of about 25 ms^{-1},

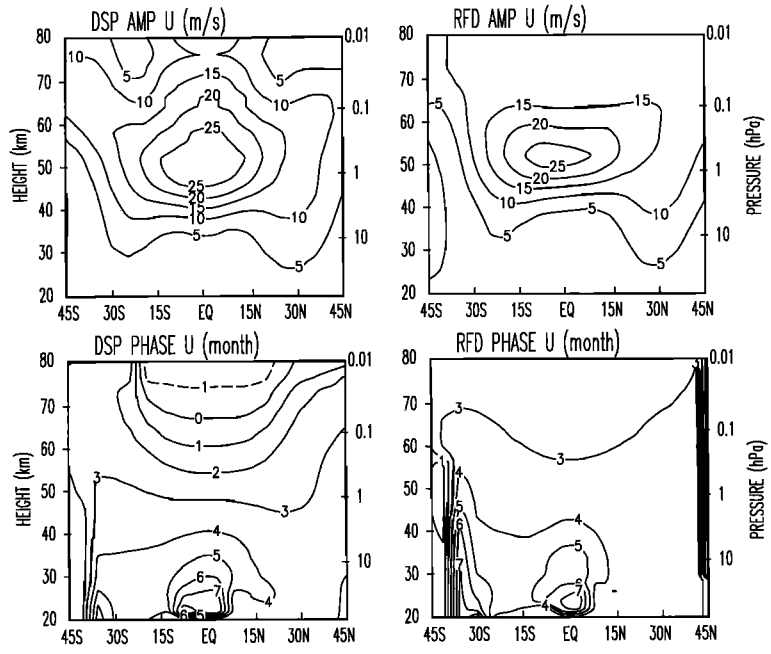

Figure 6. Amplitude of the semiannual component of the zonal mean zonal wind (ms^{-1}, top) and time of maximum westerlies (months, bottom), DSP simulation at left and RFD simulation at right. The contour interval is 5 ms^{-1} for the zonal winds and 1 month for the phases (Month 0 is January).

and decreases poleward, in qualitative accord with observations [*Hirota*, 1980; *Belmont et al.*, 1974]. The interhemispheric asymmetry of the semiannual amplitude (i.e., larger amplitude just south of the equator [*Belmont et al.*, 1974]) is, however, present only in the RFD experiment, which is consistent with the result that the easterlies are much stronger in January than in July only in the RFD experiment (Figure 5). The vertical structure of the semiannual amplitude at the equator also is different in the two experiments. The oscillation in the RFD experiment is vertically confined to the vicinity of the 1 hPa level, while the DSP semiannual amplitude is roughly constant between 45 and 55 km. In the upper stratosphere the vertical structure of the semiannual oscillation is better represented in the DSP experiment. The DSP amplitude minimum at 75 km appears to be about 10 km higher than that suggested by observations [*Hirota*, 1978; *Hamilton*, 1982]. There may be several reasons for this discrepancy. For instance, the vertical structure of the oscillation at the stratopause may be distorted by the absence of the oscillation at the mesopause [*Hirota*, 1978], which cannot be resolved because the top level in this model is approximately at 80 km. Another possibility, investigated by means of a simple sensitivity experiment to be discussed in section 4.1, is that the gravity-wave forcing in the DSP experiment may be somewhat too strong.

The different character of the phase of the two simulated oscillations is clearly illustrated in the bottom panels of Figure 6. While there is a clear downward progression of the time of the maximum westerlies in the DSP case, there is virtually no downward phase propagation of the semiannual oscillation in the RFD experiment. As expected from Figure 5, the maximum eastward DSP winds peak in April at the stratopause, while they are found in the upper mesosphere, close to the model top, about four months before, in December.

Consistent with the thermal wind balance, a temperature SAO of several degrees Kelvin is also found in both experiments. The temperature oscillation in the DSP simulation also propagates downward and displays a noticeable interannual variability (Figure 7, top panel).

The results from the RFD experiment indicate that the mechanism for the generation of the westward phase of the semiannual oscillation is captured by the model and is likely a consequence of the mean flow acceleration by the meridional advection associated with the residual mean meridional circulation. It is therefore reasonable to suppose that this effect is also present in the DSP experiment.

In the DSP simulation the mesospheric westerlies are associated with the selective transmission and dissipation of the gravity wave spectrum, a mechanism which is of course missing in the RFD experiment. At solstice, only eastward propagating gravity waves are transmitted through the stratosphere, where the winds are westward. Above the stratopause, where the wind shear changes sign, the eastward propagating gravity waves are dissipated, so producing the eastward drag in the mesosphere (positive drag in January and July in Figure 7, bottom panel). Downward propagation then follows,

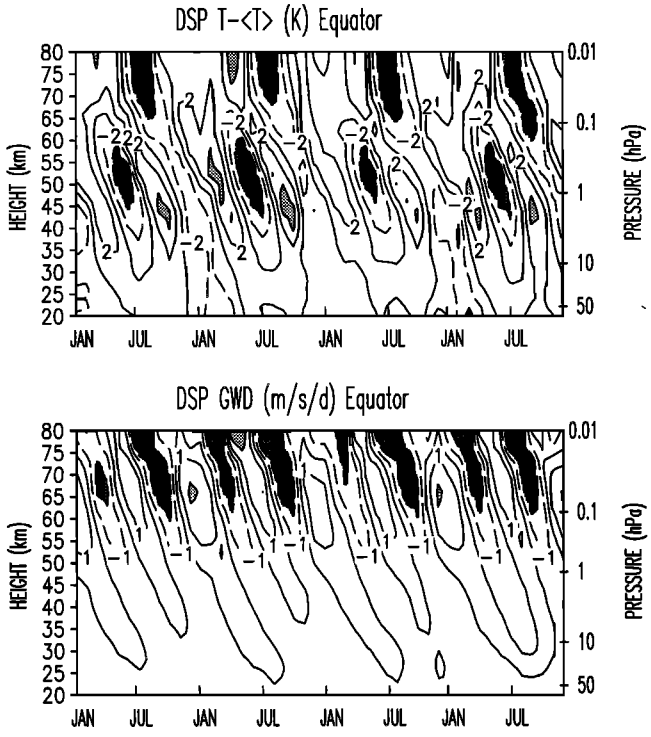

Figure 7. Time-height section of the zonal mean temperature deviation from the long-term mean (K, top) and the zonal mean zonal drag ($ms^{-1}d^{-1}$, bottom) at the equator from the DSP simulation. The contour interval is 2 K for the temperature (< -4, dark shading; > 4, light shading) and 1 $ms^{-1}d^{-1}$ for the zonal drag (< -2, dark shading; > 2, light shading).

because the largest mean flow acceleration occurs where the wind shear is largest, just below the mean flow maximum. When the strongest westerlies have reached the stratopause, the selective transmission and dissipation process is reversed. Westward traveling gravity waves propagate through the upper stratosphere, are filtered out in the mesosphere, and thus force the mesospheric easterlies. This mechanism of selective filtering of a gravity wave spectrum is well known and has been shown to produce equatorial oscillations in various idealized models (see *Andrews et al.*, [1987] for a review).

4.1. Sensitivity of Simulated SAO Westward Phase

Although the phase distribution and the enhancement of the eastward phase of the SAO simulated by the DSP experiment may be considered an improvement, over that of the RFD simulation, there are some aspects of it that are not completely satisfying. These include the lack of interhemispheric asymmetry in the semiannual amplitude distribution and the associated weak seasonal variation and pronounced downward propagation of the westward phase. Given that the westward phase of the RFD experiment is actually more realistic in this respect, it is possible that the use of an isotropic spectrum at the initial height in the DSP experiment may have produced an excess of gravity wave forcing in the westward azimuth.

To investigate this possibility in a simple and direct way, an additional 4 year simulation was performed, retaining the same configuration as in the DSP experiment, but setting the rms horizontal wind in the westward azimuth at the initial height to zero. The mean zonal wind at the equator obtained in this case (referred to as DSP.II) is shown in Figure 8 (top panel). As in the DSP simulation, a semiannual oscillation is found at the stratopause, with easterlies and westerlies propagating downward from the middle mesosphere. In the upper stratosphere, there appears to be a more uniform transition from westerlies to easterlies and an enhancement of the seasonal variation, with a stronger first cycle. Consequently, the DSP.II semiannual amplitude is slightly stronger just south of the equator at the stratopause and also decreases more rapidly with height in the mesosphere (not shown). That these changes are directly related to the gravity wave forcing is shown in the bottom panel of Figure 8, where the mean zonal gravity-wave drag at the equator is depicted. In the upper mesosphere the westward drag is clearly reduced in the DSP.II experiment, while the eastward drag is comparable in the two experiments.

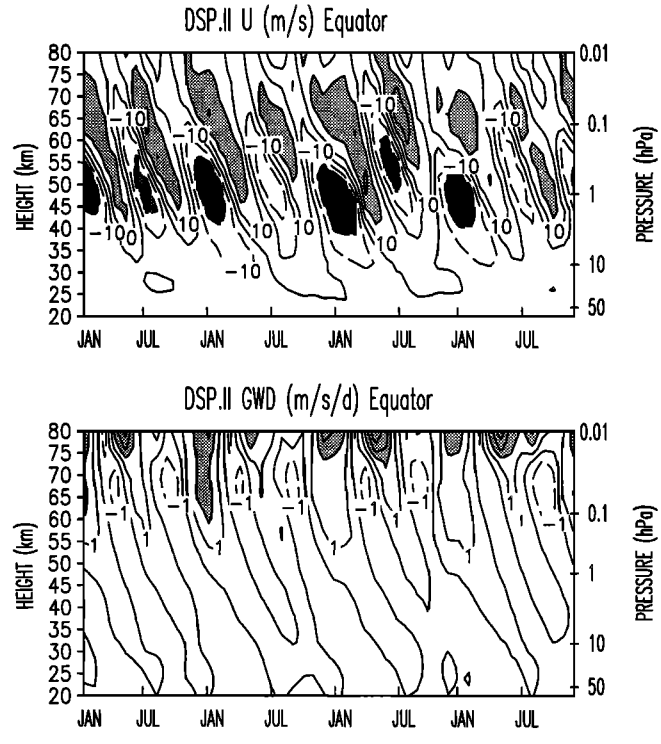

Figure 8. Time-height section of the zonal mean zonal wind (ms^{-1}, top) and zonal drag ($ms^{-1}d^{-1}$, bottom) at the equator from the DSP.II simulation. The contour interval is 10 ms^{-1} for the zonal wind (< -20, dark shading; > 20, light shading) and 1 $ms^{-1}d^{-1}$ for the zonal drag (< -2, dark shading; > 2, light shading).

5. Conclusions

Selected results of a 4-year simulation (the DSP experiment) carried out with the MA/ECHAM4 middle-atmosphere general circulation model that includes the Doppler spread parameterization have been presented and have established the feasibility of using this parameterization in GCMs. The Doppler spread parameterization [*Hines*, 1997a, b] is based on the Doppler spread theory [*Hines*, 1991a, b, c; *Hines*, 1993] and accounts for the combined effects of nonlinear interactions among the waves and dissipation associated with the onset of instability in the determination of the momentum deposition due to a continuous spectrum of upward propagating gravity waves. An additional 4 year simulation (the RFD experiment) made with MA/ECHAM4 model that used Rayleigh friction instead of the Doppler spread parameterization was performed and compared to the DSP experiment.

The results presented have demonstrated that the Doppler spread parameterization is more effective than the Rayleigh friction in reducing the magnitude of the zonal mean zonal wind in the extratropical mesosphere in January and July. This is particularly evident in the southern hemisphere in July and may be expected since the dissipation of the gravity-wave spectrum in the Doppler spread parameterization depends on vertical variations of the large-scale winds. In the upper mesosphere, where the vertical shear of the zonal wind is westward in winter, westward propagating gravity waves are strongly dissipated, thus facilitating the deceleration of the zonal mean zonal wind. This mechanism is of course not possible using Rayleigh friction, which is linearly proportional to the wind and therefore most effective only in regions where the winds are strong.

Despite these improvements, there are still noticeable biases in the simulated DSP zonal mean circulation. These include the strong westerlies in the northern hemisphere winter, presumably due to the low resolution used and to the exclusion of other dissipation processes (such as orographic gravity wave drag). Preliminary results from a recent 5 year integration with a T30 version of the current MA/ECHAM4 model, which used the Doppler Spread parameterization and an orographic gravity wave drag (based on *McFarlane* [1987]), indicate that a more realistic zonal mean circulation is obtained [*Manzini et al.*, 1997; *McFarlane and Manzini*, 1997]. A substantial cold bias is also present in the southern hemisphere winter stratosphere.

In the tropical middle atmosphere the comparison of the DSP and RFD experiments has demonstrated that both the downward propagation and the eastward phase of the simulated semiannual oscillation in the zonal mean zonal wind at the stratopause are enhanced in the DSP experiment. A more developed eastward phase in the DSP simulation is in agreement with the interpretation that gravity waves may substantially contribute to its forcing, although equatorial Kelvin waves also play a role [*Hamilton*, 1986; *Hitchman and Leovy*, 1988]. The role of equatorial planetary waves has not yet been investigated in the MA/ECHAM4 model.

When the Doppler spread parameterization is used, the simulated semiannual oscillation is found to be in part sensitive to the specification of the input gravity wave spectrum. In the DSP.II experiment, where the rms wind in the westward azimuth at the initial height has been arbitrarily set to zero, the simulated oscillation retains its basic character, while seasonal variations and the asymmetry in the downward propagation are improved. These results are consistent with the interpretation that the westward phase of the semiannual oscillation at the stratopause is forced in large part by the mean meridional advection of the summer easterlies into the winter hemisphere.

The dependence of the stratopause semiannual oscillation on the parameterized gravity wave momentum deposition seen in the MA/ECHAM4 model is consistent with the previous results of *Jackson and Gray* [1994] who found a marked improvement in the simulation of the eastward phase in the extended UGAMP GCM by introducing a single gravity wave with phase speed of 20 ms^{-1} in a *Lindzen* [1981] type gravity wave parameterization. The improvement of the simulation of the SAO therefore does not appear to be restricted to the use of only the Doppler spread parameterization.

Concerning the SAO at the stratopause, the results from the MA/ECHAM4 general circulation model are also consistent with those of *Mengel et al.* [1995], who used the Doppler spread parameterization in a two-dimensional middle-atmosphere model. They found a semiannual oscillation in the zonal mean zonal wind in the tropical mesosphere and upper stratosphere, which they attributed to the effects of gravity wave dissipation as represented by the Doppler spread parameterization.

In the tropical lower stratosphere, *Mengel et al.* [1995] found a longer period oscillation (about 20 months), with features similar to the observed quasi-biennial oscillation (QBO), but of weaker amplitude. In the present study, there appeared to be no suggestion of a realistic QBO, although very weak fluctuations (<3 ms^{-1} amplitude) on a biennial scale are present in all three simulations. These fluctuations were found to be sensitive to the specification of the surface rms wind distribution in the DSP and DSP.II experiments. In this respect, the results obtained in the present study appear to be in contrast with the findings of *Mengel et al.* [1995]. However, their simulated QBO-like oscillation was found in a two-dimensional model, which did not include midlatitude planetary waves and explicit parameterizations of physical processes usually present in a general circulation model. In addition, their QBO-like oscillation was obtained in a simulation performed using a latitudinal average of the vertical diffusion associated with the Doppler spread parameterization, an effect not included in the present experiments.

It should be noted that *Mengel et al.* [1995] only report on results with the mean and annual cycle removed, without indicating whether the QBO-like oscillation is actually producing alternating easterlies and westerlies at the equator. In a subsequent paper, *Mayr et al.* [1997] further examined the *Mengel et al.* [1995] results by means of sensitivity experiments. There it is shown that the oscillation is very sensitive to the imposed gravity-wave momentum flux and vertical diffusion, therefore putting into question the robustness of their results.

It is important to note that a somewhat idealized choice of the empirical input parameters of the Doppler spread parameterization has been used so far. Concerning the excessively strong southern hemisphere winter westerlies and the deficiencies in the summer hemisphere easterlies, the major limitation of the parameter settings used in the current model appears to be the imposition of a geographically uniform isotropic gravity wave spectrum. Although it is beyond the scope of this paper to determine the optimal parameter settings, the present results indicate, for instance, that an overall increase of the rms wind speed would improve the southern hemisphere winter by decreasing the westerlies while at the same time would worsen the northern hemisphere summer by reducing the easterlies. Consequently a seasonal variation of that parameter would have to be introduced.

A first attempt to include both the seasonal and the spatial variability associated with convective and frontal activity has been reported on by *Manzini et al.* [1997]. Those results show that an increase in the gravity wave rms wind speed proportional to the total simulated precipitation appears to improve the simulation in spring and autumn but not significantly in the southern hemisphere winter.

Clearly, the task of defining these model parameters is very difficult. Hopefully, further observations of gravity wave spectral quantities, like wind and temperature variances and propagation directions, will help constrain the DSP and other gravity wave parameterization schemes.

Acknowledgments. The authors would like to thank Lennart Bengtsson for support and encouragement, Colin O. Hines and Ted Shepherd for helpful and constructive discussions, and Ulrich Schlese and colleagues at DKRZ and MPI for technical assistance. Most of this work was carried out while N. A. McFarlane was visiting at the Max Planck Institute. E. Manzini was supported by the project "Klimavariabilität und Signalanalyse" of the Bundesministerium für Bildung und Forschung (BMBF) under grant 07VKV01/1.

References

Allen, S. J., and R. A. Vincent, Gravity wave activity in the lower atmosphere: Seasonal and latitudinal variations, *J. Geophys. Res., 100,* 1327-1350, 1995.

Andrews, D. G., J. R. Holton, and C. B. Leovy, *Middle atmospheric dynamics,* 489 pp., Academic Press, San Diego, Calif., 1987.

Belmont, A. D., D. G. Dartt, and G. D. Nastrom, Periodic variations in stratospheric zonal wind from 20 to 65 km, *Q. J. R. Meteorol. Soc., 100,* 203-211, 1974.

Belmont, A. D., D. G. Dartt, and G. D. Nastrom, Variations of stratospheric zonal winds, 20-65 km, 1961-1971, *J. Appl. Meteorol., 14,* 585-594, 1975.

Blondin, C., Research on land surface parameterization schemes at ECMWF, in *Parameterization of Fluxes Over Land Surface, ECMWF Proc.,* 285-330, Reading, England, 1989.

Boville, B. A., Sensitivity of simulated climate to model resolution, *J. Clim., 4,* 469-485, 1991.

Boville, B. A., Middle atmosphere version of the CCM2 (MACCM2): Annual cycle and interannual variability, *J. Geophys. Res., 100,* 9017-9039, 1995.

Brinkop, S., and E. Roeckner, Sensitivity of a general circulation model to parameterizations of cloud-turbulence interactions in the atmospheric boundary layer, *Tellus, 47*(A), 197-220, 1995.

Delisi, D. P., and T. J. Dunkerton, Seasonal variations of the semiannual oscillation, *J. Atmos. Sci., 45,* 2772-2787, 1988.

Dewan, E. M., and R. E. Good, Saturation and the "universal" spectrum for vertical profiles of horizontal scalar winds in the atmosphere, *J. Geophys. Res., 91,* 2742-2748, 1986.

Dümenil, L., and E. Todini, A rainfall-runoff scheme for use in the Hamburg climate model, in *Advances in theoretical hydrology, a tribute to James Dooge,* edited by J. P. O'Cane, *EGS Ser. on Hydrological Sciences, 1,* 129-157, Elsevier Press, Amsterdam, Netherlands, 1992.

Dunkerton, T. J., Theory of the mesopause semiannual oscillation, *J. Atmos. Sci., 39,* 2681-2690, 1982.

Fels, S. B., Radiative-dynamical interactions in the middle atmosphere, *Adv. Geophys., 28*(A), 277-300, 1985.

Fleming, E. L., S. Chandra, J. J. Barnett, and M. Corney, Zonal mean temperature, pressure, zonal wind and geopotential height as functions of latitude, *Adv. Space Res., 10,* 1211-1259, 1990.

Fritts, D. C., Gravity wave saturation in the middle atmosphere: A review of theory and observations, *Rev. Geophys., 22,* 275-308, 1984.

Fritts, D. C., A review of gravity wave saturation processes, effects, and variability in the middle atmosphere, *Pure Appl. Geophys., 130,* 343-371, 1989.

Fritts, D. C., and G. D. Nastrom, Sources of mesoscale variability of gravity waves, II, Frontal, convective and jet stream excitation, *J. Atmos. Sci., 49,* 111-127, 1992.

Gates, W. L., AMIP: The atmospheric model intercomparison project, *Bull. Am. Meteorol. Soc., 73,* 1962-1970, 1992.

Giorgetta, M., and M., Wild, The water vapour continuum and its representation in ECHAM4, *MPI Rep., 162,* 32 pp., Hamburg, Germany, 1995.

Hamilton, K., Rocketsonde observations of the mesospheric semiannual oscillation at Kwajalein, *Atmos. Ocean, 20,* 281-286, 1982.

Hamilton, K., Dynamics of the stratospheric semiannual oscillation, *J. Meteorol. Soc. Jpn., 64,* 227-243, 1986.

Hamilton, K., Interannual variability in the Northern Hemisphere winter middle atmosphere in control and perturbed experiments with the GFDL SKYHY general circulation model, *J. Atmos. Sci., 52,* 44-66, 1995.

Hamilton, K., R. J. Wilson, J. D. Mahlman, and L. J. Umscheid, Climatology of the SKYHI troposphere stratosphere mesosphere general circulation model, *J. Atmos. Sci., 52,* 5-43, 1995.

Haynes, P. H., C. J. Marks, M. E. McIntyre, T. G. Shepherd, and K. P. Shine, On the "Downward Control" of

extratropical diabatic circulations by eddy-induced mean zonal forces, *J. Atmos. Sci., 48,* 651-678, 1991.

Hines, C. O., The saturation of gravity waves in the middle atmosphere. Part I: Critique of linear instability theory. *J. Atmos. Sci., 48,* 1348-1359, 1991a.

Hines, C. O., The saturation of gravity waves in the middle atmosphere. Part II: Development of Doppler-spread theory, *J. Atmos. Sci., 48,* 1360-1379, 1991b.

Hines, C. O., The saturation of gravity waves in the middle atmosphere. Part III: Formation of the turbopause and the turbulent layers beneath it, *J. Atmos. Sci., 48,* 1380-1385, 1991c.

Hines, C. O., The saturation of gravity waves in the middle atmosphere. Part IV: Cutoff of the incident wave spectrum, *J. Atmos. Sci., 50,* 3045-3060, 1993

Hines, C. O., Doppler spread parameterization of gravity wave momentum deposition in the middle atmosphere. Part 1: Basic formulation, *J. Atmos. Solar Terr. Phys., 59,* 371-386, 1997a.

Hines, C. O., Doppler spread parameterization of gravity wave momentum deposition in the middle atmosphere. Part 2: Broad and quasi monochromatic spectra and implementation, *J. Atmos. Solar Terr. Phys., 59,* 387-400, 1997b.

Hirota, I., Equatorial waves in the upper stratosphere and mesosphere in relation to the semiannual oscillation of the zonal wind, *J. Atmos. Sci., 35,* 714-722, 1978.

Hirota, I., Observational evidence of the semiannual oscillation in the tropical middle atmosphere. A review, *Pure Appl. Geophys., 118,* 217-238, 1980.

Hitchman, M. H., and C. B. Leovy, Estimation of the Kelvin wave contribution to the semiannual oscillation *J. Atmos. Sci., 45,* 1462-1475, 1988.

Jackson, D.R., and L.J. Gray, Simulation of the semi-annual oscillation of the equatorial middle atmosphere using the Extended UGAMP general circulation model, *Q. J. R. Meteorol. Soc., 120,* 1559-1558, 1994.

Lindzen, R. S., Turbulence and stress owing to gravity wave and tidal breakdown, *J. Geophys. Res., 86,* 9707-9714, 1981.

Lübken, F.-J., and U. von Zahn, Thermal structure of the mesopause region at polar latitudes, *J. Geophys. Res., 96,* 20841-20857, 1991.

Manzini, E., and L. Bengtsson, Stratospheric climate and variability from a general circulation model and observations, *Clim. Dyn., 12,* 615-639, 1996.

Manzini, E., N. A. McFarlane, and C. McLandress, Middle atmosphere simulations with the ECHAM4 model: Sensitivity to the Doppler spread gravity wave parameterization, in *Gravity Wave Processes and Their Parameterization in Global Climate Models,* edited by K. Hamilton, *NATO ASI Ser. I, 50,* 367-381, 1997.

Mayr, H.G., J.G.Mengel, C.O. Hines, K.L. Chan, and N.F. Arnold, Modeling the seasonal cycle and equatorial oscillations with a parameterization of the Doppler spread gravity wave theory, in *Gravity Wave Processes and Their Parameterization in Global Climate Models,* edited by K. Hamilton, *NATO ASI Ser. I, 50,* 257-274, 1997.

McFarlane, N. A., The effect of orographically exited gravity wave drag on the general circulation of the lower stratosphere and troposphere, *J. Atmos. Sci., 44,* 1775-1800, 1987.

McFarlane, N. A., and E. Manzini, Parameterization of gravity wave drag in comprehensive models of the middle atmosphere, *Adv. Space Res.,* in press, 1997.

McFarlane, N. A., C. McLandress, and S. Beagley, Seasonal simulations with the Canadian Middle Atmosphere Model: Sensitivity to a combination of orographic and Doppler spread parameterizations of gravity wave drag, in *Gravity Wave Processes and Their Parameterization in Global Climate Models,* edited by K. Hamilton, *NATO ASI Ser. I, 50,* 351-366, 1997.

McLandress, C., Sensitivity studies using the Hines and Fritts gravity wave drag parameterizations, in *Gravity Wave Processes and Their Parameterization in Global Climate Models,* edited by K. Hamilton, *NATO ASI Ser. I, 50,* 245-255, 1997.

Medvedev, A. S., and G. P. Klassen, Vertical evolution of gravity wave spectra and the parameterization of associated wave drag, *J. Geophys. Res., 100,* 25841-25853, 1995.

Mengel, J. G., H. G. Mayr, K. L. Chan, C. O. Hines, C. A. Reddy, N. F. Arnold, and H. S. Porter, Equatorial oscillations in the middle atmosphere generated by small scale gravity waves, *Geophys. Res. Lett., 22,* 3027-3030, 1995.

Miller, M. J., T. N. Palmer, and R. Swinbank, Parameterization and influence of subgrid scale orography in general circulation and numerical weather prediction models, *Meteorol. Atmos. Phys., 40,* 84-109, 1989.

Morcrette, J. J., Radiation and cloud radiative properties in the European Centre for Medium Range Weather Forecasts forecasting system, *J. Geophys. Res., 96,* 9121-9132, 1991.

Reed, R. J., Some features of the annual temperature regime in the tropical stratosphere, *Mon. Weather Rev., 90,* 211-215, 1962.

Reed, R. J., The present status of the 26-month oscillation, *Bull. Am. Meteorol. Soc., 46,* 374-387, 1965.

Reed, R. J., Zonal wind behaviour in the equatorial stratosphere and lower mesosphere, *J. Geophys. Res., 71,* 4223-4233, 1966.

Roeckner, E., K. Arpe, L. Bengtsson, M. Christoph, M. Claussen, L. Dümenil, M. Esch, M. Giorgetta, U. Schlese, U. Schulzweida, The atmospheric general circulation model ECHAM4: Model description and simulation of present-day climate, *MPI Rep., 218,* 90 pp, Hamburg, Germany, 1996a.

Roeckner, E., J. M. Oberuber, A. Bacher, M. Christoph, and I. Kirchner, ENSO variability and atmospheric response in a global coupled atmosphere-ocean GCM, *Clim. Dyn., 12,* 734-754, 1996b.

Roeckner, E., M. Rieland, and E. Keup, Modelling of cloud and radiation in the ECHAM model, in *Cloud, radiative transfer and the hydrological cycle, ECMWF/WCRP Proc.,* 199-222, Reading, England, 1991.

Sassi, F., R. R. Garcia, and B. A. Boville, The stratopause semiannual oscillation in the NCAR Community Climate Model, *J. Atmos. Sci., 50,* 3608-3624, 1993.

Smith, S. A., D. C. Fritts, and T. E. VanZandt, Evidence for a saturated spectrum of atmospheric gravity waves, *J. Atmos. Sci., 44,* 1404-1410, 1987.

Tiedtke, M., A comprehensive mass flux scheme for cumulus parameterization in large-scale models, *Mon. Weather Rev., 117,* 1779-1800, 1989.

Williamson, D. L. and P. J. Rasch, Water vapour transport in the NCAR CCM2, *Tellus, 46*(A), 34-51, 1994.

E. Manzini, Max Planck Institut für Meteorologie, Bundesstrasse 55, 20146 Hamburg, Germany. (e-mail: manzini@dkrz.de)

N. A. McFarlane, Canadian Centre for Climate Modelling and Analysis, Atmospheric Environment Service, University of Victoria, P.O. Box 1700, Victoria, B.C. V8W 2Y2, Canada. (email: Norm.McFarlane@ec.gc.ca)

C. McLandress, University of Washington, Department of Atmospheric Sciences, Box 351640, Seattle, WA 98195-1640. (email: charles@atmos.washington.edu)

(Received September 18, 1996; revised March 31, 1997; accepted April 7, 1997.)